ANALYSIS OF DELTA WING VORTICAL SUBSTRUCTURES USING DETACHED-EDDY SIMULATION

Anthony Mitchell*, Scott Morton† and James Forsythe‡
United States Air Force Academy, Department of Aeronautics
2410 Faculty Drive, USAF Academy, CO 80840, USA.

ABSTRACT

An understanding of the vortical structures which comprise the vortical flowfield around slender bodies is essential for the development of highly maneuverable and high angle of attack flight. This is primarily due to the physical limits these phenomena impose on aircraft and missiles at extreme flight conditions. Demands for more maneuverable air vehicles have pushed the limits of current CFD methods in the high Reynolds number regime. Simulation methods must be able to accurately describe the unsteady, vortical flowfields associated with fighter aircraft at Reynolds numbers more representative of full scale vehicles. It is the goal of this paper to demonstrate the ability of Detached-Eddy Simulation, a hybrid RANS-LES method, to accurately model the vortical flowfield over a slender delta wing at Reynolds numbers above 1 million. Detached-Eddy Simulation has successfully predicted the location of the vortex breakdown phenomenon and the goal of the current effort is to analyze and assess the influence of vortical substructures in the separating shear layers which roll up to form the leading-edge vortices. Very detailed experiments performed at ONERA using 3-D Laser Doppler Velocimetry measurement will be used to compare simulations utilizing DES turbulence models. The computational results provide novel insight into the formation and impact of the vortical substructures in the separating shear layers on the entire vortical flowfield.

INTRODUCTION

The delta wing flowfield is dominated by vortical structures, the most prominent called leading-edge vortices. As angle of attack increases, these leading-edge vortices experience a sudden disorganization, known as vortex breakdown, which can be described by a rapid deceleration of both the axial and swirl components of the mean velocity and, at the same time, a dramatic expansion of the vortex core. Substantial theoretical, experimental and computational research has focused on the characteristics of leading-edge vortices and vortex breakdown.[1-8] However, limited efforts have sought to understand the separating shear layers which roll up to form the leading-edge vortices.

Various researchers have observed discrete vortical substructures in the shear layers and the resulting data have taken on two contrasting descriptions: temporal substructures (rotating around the leading-edge vortex)[9-12] and spatially stationary substructures (spatially fixed around the periphery of the leading-edge vortex).[13-20] Additionally, many of these researchers have hypothesized about the type of instability which results in the formation of the vortical substructures. None of these hypotheses has been universally accepted or proven. The most popular hypothesis[9,11,14,15,18,19] proposes that the substructures develop in a manner similar to the Kelvin-Helmholtz instability or that of a two-dimensional shear layer instability described by Ho and Huerre.[21] Another hypothesis suggests that the substructures originate from transversal perturbations along the leading edge of the wing induced by the interaction between the separating shear layer and the

---

* Major, USAF. Asst. Prof. of Aeronautics. Senior Member AIAA.
† Major, USAF. Assoc. Prof. of Aeronautics. Assoc. Fellow AIAA.
‡ Major, USAF. Assoc. Prof. of Aeronautics. Senior Member AIAA.

Report Documentation Page

Form Approved
OMB No. 0704-0188

1. REPORT DATE	2. REPORT TYPE	3. DATES COVERED
00 JAN 1997	**N/A**	**-**

4. TITLE AND SUBTITLE	5a. CONTRACT NUMBER
Analysis Of Delta Wing Vortical Substructures Using Detached-Eddy Simulation	5b. GRANT NUMBER
	5c. PROGRAM ELEMENT NUMBER
6. AUTHOR(S)	5d. PROJECT NUMBER
	5e. TASK NUMBER
	5f. WORK UNIT NUMBER
7. PERFORMING ORGANIZATION NAME(S) AND ADDRESS(ES) **United States Air Force Academy, Department of Aeronautics 2410 Faculty Drive, USAF Academy, CO 80840, USA**	8. PERFORMING ORGANIZATION REPORT NUMBER
9. SPONSORING/MONITORING AGENCY NAME(S) AND ADDRESS(ES)	10. SPONSOR/MONITOR'S ACRONYM(S)
	11. SPONSOR/MONITOR'S REPORT NUMBER(S)

12. DISTRIBUTION/AVAILABILITY STATEMENT
Approved for public release, distribution unlimited

13. SUPPLEMENTARY NOTES
See also ADM001662., The original document contains color images.

14. ABSTRACT

15. SUBJECT TERMS

16. SECURITY CLASSIFICATION OF:			17. LIMITATION OF ABSTRACT	18. NUMBER OF PAGES	19a. NAME OF RESPONSIBLE PERSON
a. REPORT	b. ABSTRACT	c. THIS PAGE			
unclassified	**unclassified**	**unclassified**	**UU**	**12**	

Standard Form 298 (Rev. 8-98)
Prescribed by ANSI Std Z39-18

secondary vortices.[10,20] Washburn and Visser[17] suggested the substructures are generated by non-viscous instabilities in the shear layer and that their formation is governed by the transverse flow of the leading-edge vortices. Yet another hypothesis postulates that a longitudinal instability associated with the curvature of the separating shear layer is at the origin of the substructures.[18] Some experimentally-based hypotheses indicate that the instabilities are generated by the presence of small amplitude surface waves in the water tunnel[10] or are associated with vibrations in a wind tunnel.[15]

Advances in non-intrusive experimental measurement techniques have enabled more detailed analysis of the vortical flowfield and the separating shear layers forming the leading-edge vortices around a delta wing. Three-dimensional Laser Doppler Velocimetry (LDV) flowfield measurements were acquired in ONERA's 1.4m x 1.8m subsonic wind tunnel around a sharp-edged delta wing model.[22-24] These results provide new insight into the phenomenon through precisely measured details of the characteristics and path of the vortical substructures around the leading-edge vortex core. However, the experimental results provide a finite amount of flowfield information. For these reasons, an accurate CFD prediction of the flowfield over a slender delta wing at high angles of attack and high Reynolds numbers is necessary to further analyze and better understand the separating shear layers that roll up to form the primary and secondary vortices.

While advances have taken place in areas such as grid generation and fast algorithms for solution of systems of equations, CFD has remained limited as a reliable tool for prediction of inherently unsteady flows at flight Reynolds numbers. Current engineering approaches to prediction of unsteady flows are based on solution of the Reynolds-averaged Navier-Stokes (RANS) equations. The turbulence models employed in RANS methods necessarily model the entire spectrum of turbulent motions. While often adequate in steady flows with no regions of reversed flow, or possibly exhibiting shallow separations, it appears inevitable that RANS turbulence models are unable to accurately predict phenomena dominating flows characterized by massive separations. Unsteady, massively-separated flows are characterized by geometry-dependent and three dimensional turbulent eddies. These eddies, arguably, are what defeats RANS turbulence models, of any complexity.

To overcome the deficiencies of RANS models for predicting massively separated flows, Spalart et.al.[25] proposed Detached-Eddy Simulation (DES) with the objective of developing a numerically feasible and accurate approach combining the most favorable elements of RANS models and Large Eddy Simulation (LES). The primary advantage of DES is that it can be applied at high Reynolds numbers as can Reynolds-averaged techniques, but also resolves geometry-dependent, unsteady three-dimensional turbulent motions as in LES. DES predictions to date have been favorable, forming one of the motivations for this research. The specific aim of this work is to apply and assess DES with respect to vortical substructures in the separating shear layers over slender delta wings at high Reynolds number.

EXPERIMENTAL MODEL AND WIND TUNNEL

The delta wing model in this study has a 70° sweep angle and root chord (c) of 950mm. It has a wingspan of 691.5 mm at its trailing edge, is 20mm thick, and is beveled on the windward side at an angle of 15° to form sharp leading edges (see Fig. 1). All of the data presented in this paper was acquired in ONERA's 1.4m x 1.8m subsonic wind tunnel (F2) at test conditions of $\alpha = 27°$ and $U_\infty = 24$m/s ($Re_c = 1.56 \times 10^6$). Due to the relative symmetry of the flowfield over the leeward surface of the delta wing, only the portside flowfield was examined. Details of the model, the wind tunnel and LVD system are specified in References 23 and 24.

EXPERIMENTAL ERROR AND ACCURACY

In ONERA's F2 wind tunnel, the relative freestream velocity, $\Delta U_\infty/U_\infty$, is estimated to have an accuracy of ±1%, while the mean intensity of turbulence is approximately 0.1%. The model was mounted on a sting with a horizontal support and flexible joint for adjusting the angle of attack, with an accuracy of ±0.05°. The horizontal support was manipulated in height along a vertical column so as to maintain the model close to the center axis of the test section. The model was mounted in the test section with no yaw angle with respect to the freestream flow (estimated accuracy of ± 0.1°).[23,24] The LDV system installed in F2 utilizes two 15W argon lasers as the sources of light in a forward scattering mode. The global accuracy of the LDV system is estimated to have a relative error, $\Delta U/U$, of less than 1.5% assuming an absolute error of the angle between the velocity vector and a horizontal reference of 0.5°. Therefore the estimated accuracy of the magnitude of the

velocity is ±1m/s and the direction of the velocity vector is ±1°.[26]

EXPERIMENTAL RESULTS

Four LDV planes perpendicular to the leeward surface of the wing at X/c = 0.53, 0.63, 0.74 and 0.84 were explored. These planes correspond to a region where the leading-edge vortex was well developed, a zone just upstream of the vortex breakdown location, a zone downstream of the vortex breakdown location, and finally a region further downstream where the flow was fully turbulent. Each perpendicular measurement mesh consists of approximately 1400 points located between $0.4<Y/b<1.1$ on the portside of the wing, evenly spaced at 5 mm intervals.

The measurements demonstrate a strong, jet-like, acceleration of the flow along the vortex core upstream of vortex breakdown (X/c = 0.65) with values of $U/U_\infty \geq 3.5$. There is an abrupt deceleration of the axial velocity component to a stagnation point (vortex breakdown location), which is followed by a zone of recirculation and a sizeable increase in the diameter of the vortex core. The post breakdown region has a wake-like axial velocity profile. Components of vorticity are calculated from the measured mean velocity components using a central differencing scheme to evaluate the derivatives. Figure 2 represents the axial component of vorticity ($\Omega_x = \partial W/\partial y - \partial V/\partial z$) in each perpendicular plane. These traces reveal two highly rotational zones in the flowfield: (1) the vortex core with a strong negative vorticity; (2) regions of positive vorticity near the leading edge, along the suction surface of the wing, which represent the secondary vortex. Additionally, multiple substructures, rotating in the same direction as the vortex core, are clearly defined in the time-averaged data and confirm the observations of the existence of spatially stationary substructures. It is clear from the dissipation of the vorticity in the vortex core in Figures 2c and 2d that vortex breakdown has occurred. However, the vortical substructures are still present in the flowfield around the vortex core.

Due to the large spacing interval between the perpendicular planes of data presented in Fig. 2, a second series of experiments was conducted to acquire data from 12 perpendicular planes over the same region of the wing. These perpendicular planes were situated at X/c = 0.53, 0.58, 0.61, 0.63, 0.65, 0.67, 0.69, 0.72, 0.74, 0.76 and 0.84. The data were acquired using the same measurement meshes as the data shown in Fig. 2, although the delta wing model was rotated around its chord line by the addition of a wedge between the windward surface of the delta wing model and the sting. The effective incidence angle of the model with respect to the freestream velocity of the wind tunnel was maintained by simultaneously maneuvering the angles of the sting's elbow joints. This rotation of the model caused the time-averaged vortex breakdown location to shift upstream approximately 100mm (10.5% of the chord). This was the only observed modification to the flowfield as a result of the model's rotation and the results remained within the outliers of the observed instantaneous breakdown locations for both configurations. The new, more finely probed, volume of data constitutes an important data base for interpolation across the entire flowfield.

The results shown in Fig. 3 demonstrate the evolution of the discrete substructures of vorticity around the vortex core. The substructures appear to roll around the vortex core as they evolve in the downstream direction. The magnitude of the axial component of vorticity in each of the substructures is of the same order of magnitude as that measured in the vortex core. One also observes a decrease in the magnitude of the axial component of vorticity proportional to the increase in the longitudinal distance (X/c). This trend indicates the presence of a local instability near the leading edge, which is generating the substructures. Therefore, it is proposed that the substructures are formed near the leading edge and are subsequently entrained downstream by both the axial velocity of the flow and the rotational velocity of the leading-edge vortex. It is interesting to note that the substructures follow a helical trajectory around the vortex core and the spacing (frequency) between the substructures appears relatively constant, confirming the observations of Washburn and Visser.[17] Additionally, the substructures remain coherent even in the post-breakdown region of the flowfield.

Figure 4 illustrates the three-dimensional flowfield developing around the delta wing. This image was computed by interpolating the data between the various perpendicular planes of measurements. The first two planes, at X/c = 0.53 and 0.58, are shown. The rest of the data represents various stream ribbons, initiated at the center of the substructures in the first perpendicular plane, which pass through the centers of the subsequent substructures. The values indicated on the stream ribbons represent the axial component of vorticity. These stream ribbons

represent the helical trajectory of the substructures around the vortex core with constant spacing. As observed in Fig. 4, there is a decrease in the magnitude of the axial component of vorticity proportional to the increase in the longitudinal distance.

There are some discontinuities in the results presented in Fig. 4, which are likely due to problems associated with an interpolation over relatively large axial distances. In spite of these shortcomings, this approach facilitates the analysis of the substructures' trajectories and the global characteristics in the axial component of vorticity.

The ensemble of these 3-D LDV results confirms the formation and existence of co-rotating, stationary substructures in the separating shear layers which form the leading-edge vortices. The current data does not permit a precise evaluation of the instability mechanism responsible for the creation of the substructures. However, the results do point toward the existence of convective instabilities near the leading edge. These detailed experimental results will serve as a validation test case for the computational studies and analysis that should provide more precise flowfield details in the vicinity of the leading edge. Computational results are needed to confirm or disprove the many instability-related hypotheses observed experimentally. Additionally, computational results will provide further insight about the interaction of the substructures and the leading edge vortex and the influence of the substructures on the vortex breakdown location.

NUMERICAL METHOD

In this section a brief description of the numerical method is provided with full details of the computational scheme and the solution method presented[27]. Solutions were obtained for a freestream velocity of 24 m/s, an angle of attack of 27 deg, and a freestream pressure and temperature resulting in a Reynolds number of 1.56×10^6. The numerical simulation matched the angle of attack, Reynolds number, and Mach number of the wind tunnel experiments[22-24] previously described. Solutions are computed using the commercially-available solver Cobalt. Cobalt is an unstructured finite-volume method developed for solution of the compressible Navier-Stokes equations with details of the approach described in Ref. 27. The method is a cell-centered finite-volume approach applicable to arbitrary cell topologies including hexahedrals, prisms, and tetrahedra. The spatial operator uses an exact Riemann solver, least-squares gradient calculations using QR factorization to provide second-order accuracy in space, and TVD flux limiters to limit extremes at cell faces. A point implicit method using analytic first-order inviscid and viscous Jacobians is used for advancement of the discretized system. A Newton sub-iteration scheme is employed to improve time accuracy.

Turbulence Models

Cobalt has several choices of turbulence models including Spalart Allmaras (SA)[25] RANS, as well as DES based on SA.[28] The SA-DES hybrid model was found to be a suitable method for the current study by Morton et. al.[29] The following sub-sections describe the turbulence model used in the current work, and also provide references for more detailed descriptions.

Spalart-Allmaras Turbulence Model

The Spalart-Allmaras[25] one equation turbulence model solves a single partial differential equation for a working variable related to the turbulent viscosity. The differential equation is derived by using empiricism, arguments of dimensional analysis, Galilean invariance, and selected dependence on the molecular viscosity.[25] The model includes a wall destruction term that reduces the turbulent viscosity in the laminar sublayer and the log layer. Details of the model implementation and all coefficients are given in in Ref. 29.

Detached-Eddy Simulation

The DES model was originally based on the Spalart-Allmaras one equation RANS turbulence model (discussed above, with a more detailed presentation in Ref. 29). The wall destruction term is proportional to the square of the modified eddy-viscosity divided by the distance to the nearest wall $(\tilde{n} / d)^2$. When this term is balanced with the production term $\hat{S}$, the eddy viscosity becomes proportional to $\hat{S}d^2$. The Smagorinski LES model varies its sub-grid-scale (SGS) turbulent viscosity with the local strain rate, and the grid spacing described by $n_{SGS} \propto \hat{S}\Delta^2$, where $\Delta = \max(\Delta x, \Delta y, \Delta z)$. If d is replaced with Δ in the wall destruction term, the S-A model will act as a Smagorinski LES model. To exhibit both RANS and LES behavior, d in the SA model is replaced by

$$\tilde{d} = \min(d, C_{DES}\Delta), \quad C_{DES} = 0.65$$

When $d << \Delta$, the model acts in a RANS mode and when $d >> \Delta$ the model acts in a Smagorinski LES mode. Therefore, the model switches into LES mode when the grid is locally refined. DES was implemented in an unstructured grid method by Forsythe et. al.[30] They determined the C_{DES} constant could be 0.65, consistent with the structured grid implementation of Shur et. al.[31], when the grid spacing Δ was taken to be the longest distance between the cell center and all of the neighboring cell centers. All simulations in this study use the SA-DES hybrid RANS-LES turbulence model.

Grid Generation

Grids were developed using the software programs Gridtool[32], to develop the surface point distributions and background sources, and VGRIDns[33] to grow the volume grid. First, a baseline grid was created with concentration of points near the surface in the viscous region and concentration of points in the LES focus region of the vortex core by the use of Gridtool's line sources. The outer dimensions of the domain were -10m<X<10m (streamwise), 0<Y<5m (spanwise), and -5m<Z<5m (surface normal), where the root chord of the delta wing is 0.95m and the apex of the delta wing is at the origin. A half-span assumption was made for all grids generated. Next, alternate grids were produced by changing a grid control parameter in VGRIDns that modifies the distribution of points outside the viscous region consistently by the scale factor *ifact*. This approach was used to create four semi-span grids of 1.2 (Coarse Grid), 2.7 (Medium Grid), 6.7 (Fine Grid), and 10.7 million cells (Real Fine Grid). Each grid in the series is refined in all three coordinate directions by a factor of $1/\sqrt{2}$ from the previous grid in the series. Results from the first three grids were presented in Ref. 30 with a preliminary assessment. The current work adds the next refinement in the grid series (10.7 million cells) and also presents a more complete analysis of the set of grids when coupled with DES in comparison with the experiments.

Another important grid technology that is particularly well suited for DES is adaptive mesh refinement (AMR). Pirzadeh[34] presented a method based on a tetrahedral unstructured grid technology developed at NASA Langley Research Center with application to two configurations with vortex dominated flowfields. The large improvement of the adapted solutions in capturing vortex flow structures over the conventional unadapted results was demonstrated by comparisons with wind tunnel data. Pirzadeh showed the numerical prediction of these vortical flows was highly sensitive to the local grid resolution and he also stated that grid adaptation is essential to the application of CFD to these complicated flowfields. His most successful computations were performed using an inviscid method due to the inadequacies of standard turbulence models in computing these complicated flowfields.

Pirzadeh's method is applied to the ONERA delta wing configuration in the current study. A steady-state flow solution was computed for a grid with surface resolution between the coarse and medium grids described above, and then was used to create an AMR grid by eliminating all cells within an iso-surface of vorticity at a particular level. The grid was then grown inside of the iso-surface with an *ifact* of 0.5. This procedure was performed twice to create a vortex core and shear layer with $1/4^{th}$ the cell sizes (in all coordinate directions) of the original grid. The new grid was then used to compute unsteady detached-eddy simulations of the flowfield.

All of the grids in this study consist of an inner region of approximately 13 layers of prisms for the boundary layer, with a wall normal spacing in viscous wall units less than 1, and an outer region of tetrahedra. The prism dimensions on the surface were a factor of approximately 200 times larger than the wall normal dimension for all grids.

Figures 5-7 depict cross-planes of the coarse, real fine, and AMR grids at four chord-wise stations, X/c=0.53, 0.63, 0.74, 0.84. It is apparent from Figures 5 and 6 that a consistent grid refinement has occurred with very little emphasis on the vortex core or shear layer. In contrast, the AMR grid depicted in Fig. 7 shows a concentration of points in the vortex core and leading-edge shear layer regions with cell sizes smaller than even the Real Fine Grid of Fig. 6. It should be noted that the shear layer loses resolution for the chord-wise stations of 0.74 and 0.84. Fig. 8 depicts a downward look on a plane passing through the surface of the delta wing grid. The left side is the Real Fine Grid and the right side is the AMR grid. It is apparent the Real Fine Grid has refined cells outboard of the leading-edge in a region that, arguably, has little impact on the solution. It is also clear that the trailing-edge region is much more refined in the real fine grid, making it superior to the AMR grid for resolving the unsteady wake region eminating from the blunt trailing edge.

COMPUTATIONAL RESULTS

A systematic time-step and Newton sub-iteration study was presented in Ref. 29 for the medium grid. The study demonstrated that three Newton sub-iterations and a time step, non-dimensionalized by the freestream velocity and root chord, of 0.0025 was sufficient. As the grid is coarsened or refined by *ifact*, the time step was also changed in a consistent manner.

Typical simulations were run for 10,000 iterations, starting from freestream conditions, and time averages were computed starting after the 2,000th iteration to eliminate transients. Figures 9a-e show a top-view of the delta wing for the five grids discussed previously. An iso-surface of vorticity magnitude colored by the spanwise-vorticity component is displayed for each of the grids. It is apparent in Figures 9a-d that consistent grid refienement provides a significant increase in the number of flowfield structures resolved. In the pre-breakdown region of the vortex core, substructures winding around the core are observed as the grid is refined. Also, there is a significant increase in the number of structures observed in the region of the core, post-breakdown, as the grid is refined. Trailing-edge spanwise vortical structures begin to be resolved as the grid is refined, and for the Real Fine Grid, 3-D structures eminating from the blunt trailing edge that transition to these spanwise coherent vortices are also captured. The trailing-edge coherent vortices also have an effect on the leading-edge shear layer, creating an instability at the leading-edge that propogates forward as more of the trailing-edge vortices are resolved.

The AMR grid depicted in Fig 9e displays some significant differences in the pre-breakdown region. The vortical substructures are very coherent relative to the other grids and persist even downstream of the breakdown position. The trailing-edge vortices are evident but the coarseness of the grid in this region impedes the propogation of these coherent structures downstream. The lack of the leading-edge instability related to the trailing-edge coherent structures may be due to the decrease in shear layer resolution for the AMR grid, post-breakdown, discussed above. Consistent with the fact that the core of the vortex is even more refined than the Real Fine Grid, there is a tremendous amount of three-dimensional structures in the region of the core, post-breakdown.

Comparison with Experimental results

In order to compare the computational data with the experimental results, numerical planes of axial vorticity, perpendicular to the leeward surface of the wing at X/c = 0.53, 0.63, 0.74 and 0.84 are analyzed. These planes correspond to the experimentally explored regions of the flowfield shown in Fig. 2. Fig. 10 depicts the results of instantaneous axial vorticity for the Real Fine Grid DES simulation. Fig. 11 depicts the results for the AMR DES simulation.

As with the experimental results in Fig. 2, the computational data in both Figs. 10 and 11, depict multiple vortical substructures, rotating in the same direction as the vortex core. Additionally, the vortical substructures exist in the flowfield around the vortex core both upstream and downstream of the vortex breakdown location, just as they were measured experimentally. There are, however, significant differences between the data shown in Figs. 10 and 11. In Fig. 10, the Real Fine Grid solution, it appears as if the axial vorticity is spread rather evenly throughout the shear layer as it separates from the leading edge and rolls around the leading-edge vortex. In Fig. 11, the AMR solution, the axial vorticity in the separating shear layer appears to be grouped in more clearly identifiable vortical substructures. The AMR DES simulation results are much more comparable to the experimental data shown in Figs. 2 and 3.

As previously discussed, the grid resolution has a significant impact on the flow separating from the trailing edge of the delta wing. The fluctuation of this flow has an upstream influence on the shape, direction and frequency of the substructures in the shear layer and therefore dramatically impact the cross-plane data shown in Fig. 10. Animation of the solution shows the substructures separating from the leading edge and then rotating around the vortex core in a temporal manner as was observed by a number of experiments and computations, typically at lower Reynolds numbers.[9-11] Therefore, in the instantaneous cross-planes, the axial velocity is smeared throughout the shear layer.

In Fig. 11 and in animations of the solution, the AMR DES solution has a significantly different trailing-edge flow pattern and a spatially stationary vortical substructure configuration that more closely mimics experimental observations in References 13-20. Because the substructures are spatially stationary like

those in the experiments, the cross-planes of axial vorticity reveal substructures in the shear layer that closely correlate to those observed in Fig. 2.

The data in Figs. 9e and 11 demonstrates that the numerical substructures follow a helical trajectory around the vortex core and the spacing between the substructures appears relatively constant, again corresponding to the experimental results and observations by Washburn and Visser[17]. The substructures remain coherent even in the post-breakdown region of the flowfield; however, the grid resolution in the outer shear layer near the trailing edge deteriorates in the current grid and must be corrected to fully capture the phenomena.

In the experimental results shown in Figs. 2 and 3, it is difficult to follow the trajectory of a specific substructure for a complete revolution around the vortex core because the substructures are either entrained into the vortex core or are dispersed as they approach the trailing edge of the wing. Fig. 4 was used to more clearly identify the numerous half-rotations of the vortical substructures, which allow one to define the trace of helical trajectories. The trace of a helix is defined as $L/2\pi r$; where L is the longitudinal distance for one rotation and r is the radius of the helix. In Fig. 4, the substructures complete a half-rotation over a distance of 200 to 250mm and have a radius of approximately 60mm. Therefore the trace of the helix in the experimental results is between 1.06 and 1.32 and is shown in Table 1.

	Helix Trace ($L/2\pi r$)
ONERA experimental results	1.06 - 1.32
DES results - AMR grid	1.19

Table 1: Comparison of experimental and computational substructure helix traces.

From computational results using the AMR grid, Fig. 12, it was similarly difficult to follow the trajectory of a substructure for a complete revolution around the vortex core. However, trajectories were easily identified over approximately one third of a rotation. Therefore the longitudinal distance, L = 75mm, and the helix radius, r = 28mm, were acquired from 129º of trajectory. The trace of the helix in the computational results was 1.19 as shown in Table 1. The close correlation of the traces of the substructures between the experimental results and the DES solutions shown in Table 1 is another indication of the accurate predictive capabilities of this DES method for vortical and highly separated flows. It should be noted that the theory of physical deformities on the leading-edge of wind/water tunnel models creating the substructures is inconsistent with the smooth surface grid used in the computations.

It is rather disconcerting that the refined mesh in the trailing-edge region of the Real Fine Grid produces instabilities inconsistent with the experiments, whereas the coarser AMR trailing-edge grid is consistent with the experiments. This could indicate a Reynolds number effect associated with the trailing-edge vortices. For higher Reynolds numbers, as the grid is refined, more and more three-dimensional structures will be resolved in the trailing-edge region that destroy the coherence of these trailing-edge vortices, minimizing their upstream effects on the leading-edge shear layer. This hypothesis can be verified by modifying the AMR grid with a significant increase in the number of cells in the trailing-edge wake region. As the wake region is refined, first the coherent trailing-edge structures should be captured, and then weakened by additional three-dimensional structures.

CONCLUDING REMARKS

The experimental and computational results confirm the formation and existence of spatially stationary, co-rotating, substructures in the shear layers that form the leading-edge vortices over slender delta wings at high angles of attack. The 3-D LDV data and time-accurate CFD simulations characterize the structure and path of these substructures around the leading-edge vortex cores - demonstrating their origin along the leading edges and their helical trajectories around the leading-edge vortices. However, the instability mechanism responsible for the creation of the substructures is still not well understood, hence, the need for high resolution, time-accurate computational results. The Detached-Eddy Simulation RANS-LES model was able to accurately resolve these substructures but was tied significantly to the choice of grid density due to its LES nature. It has been hypothesized that the two different types of substructures observed, one stationary and the other time varying, may be tied to a trailing-edge Reynolds number effect. Further analysis is necessary to completely understand the grid requirements to capture the phenomena and the mechanism that creates these substructures.

Acknowledgements

The authors would like to express appreciation to Dr Shahyar Pirzadeh for his help producing adaptively refined meshes, as well as his enlightened discussions, during this work. The authors would also like to thank AFOSR for funding this project under the direction of Dr John Schmisseur, and the Maui High Performance Computing Center for their generous support of computational hours.

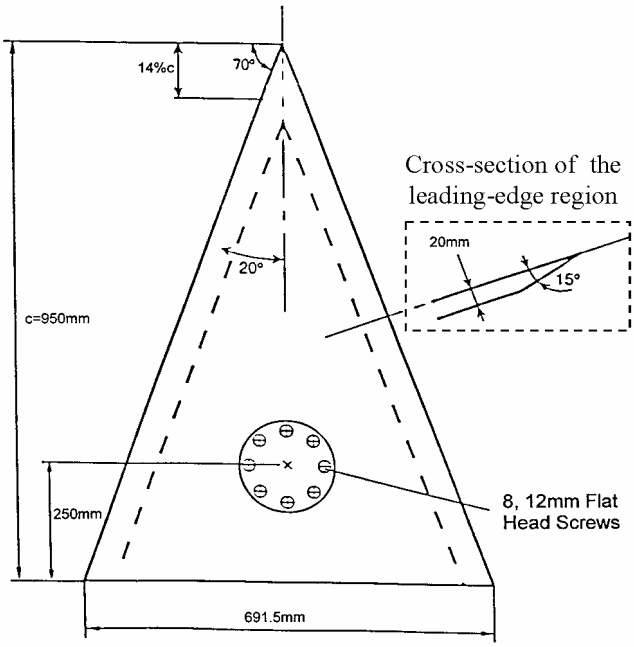

Fig. 1: Experimental delta wing model configuration.

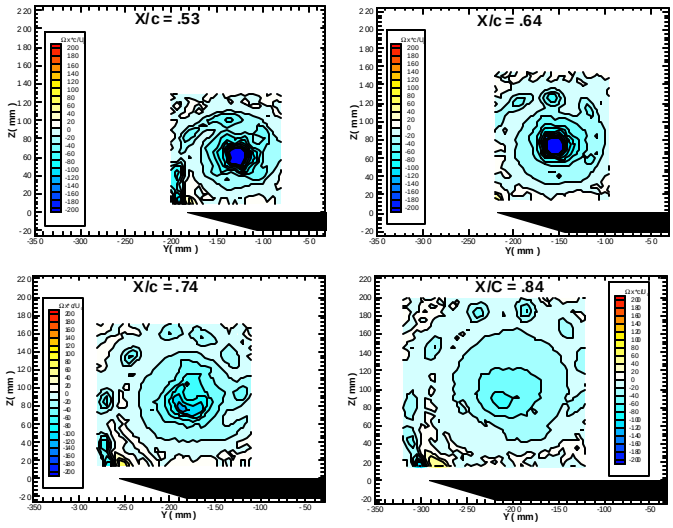

Fig. 2: LDV results showing the axial vorticity (Ω_x c/U_∞) at α = 27º and U_∞ = 24 m/s (a) X/c = 0.53 (500mm) (b) X/c = 0.63 (600mm) (c) X/c = 0.74 (700mm) (d) X/c = 0.84 (800mm).

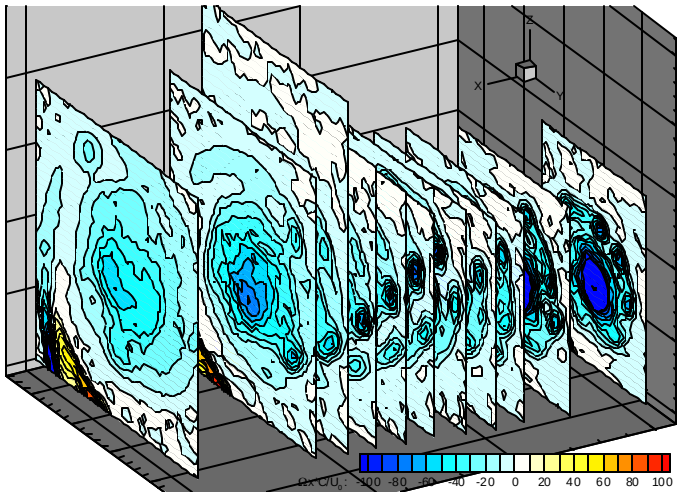

Fig. 3: LDV results of axial vorticity measured in 14 different planes perpendicular to the leeward surface of the 70° delta wing at α = 27° and Re_c = 1.56x10^6 demonstrating the existence and form of the vortical substructures. (Freestream velocity from right to left.)

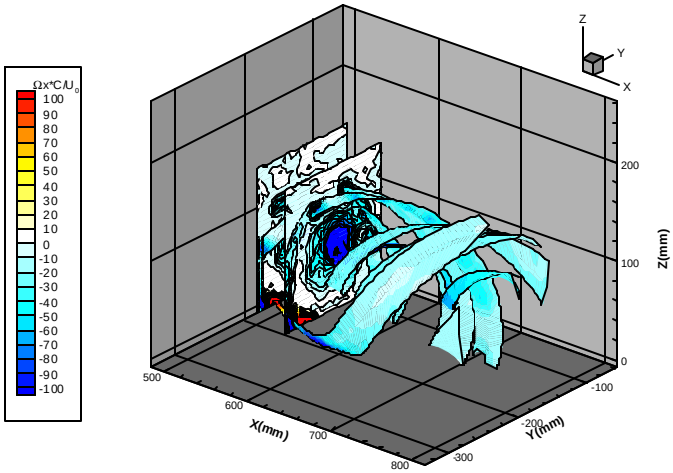

Fig. 4: LDV results. Interpolated stream ribbons following the vortical substructures around the vortex core showing values of the axial vorticity (Ω_x c/U_∞) at α = 27° and Re_c = 1.56x10^6. (Freestream velocity from left to right.)

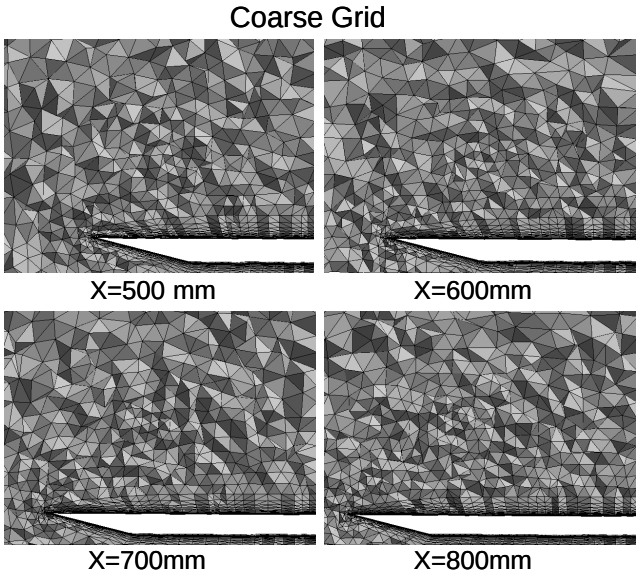

Fig. 5: Cross-planes of the coarse grid (1.2M cells) at four chord-wise stations.

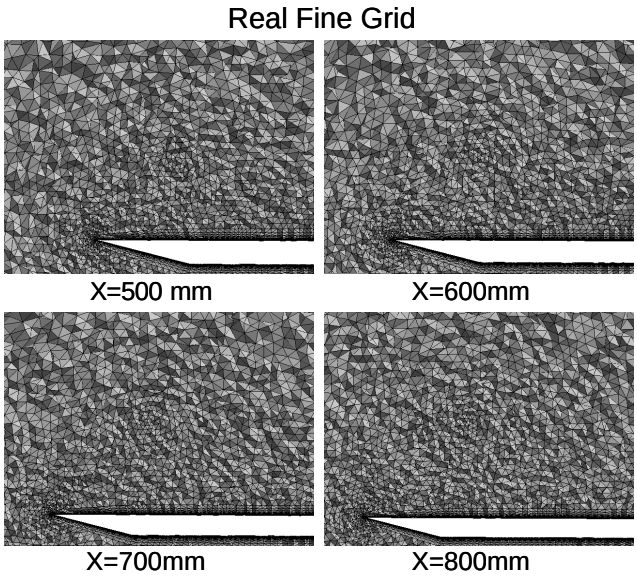

Fig. 6: Cross-planes of the real fine grid (10.7M cells) at four chord-wise stations.

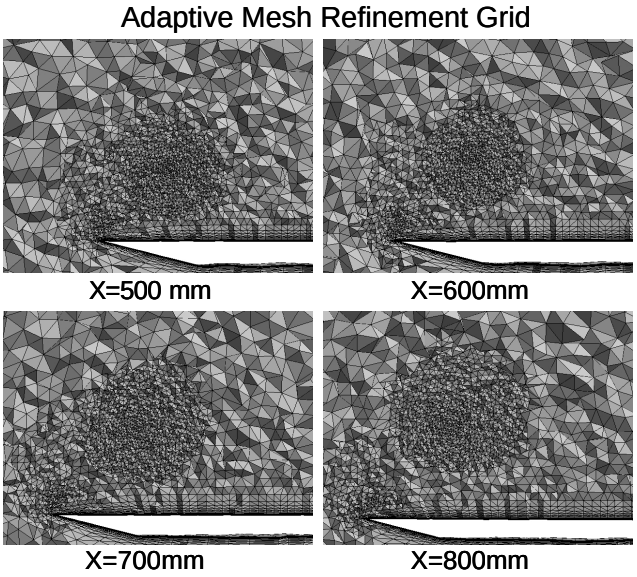

Fig. 7: Cross-planes of the adaptive mesh refinement grid (3.2M cells) at four chord-wise stations.

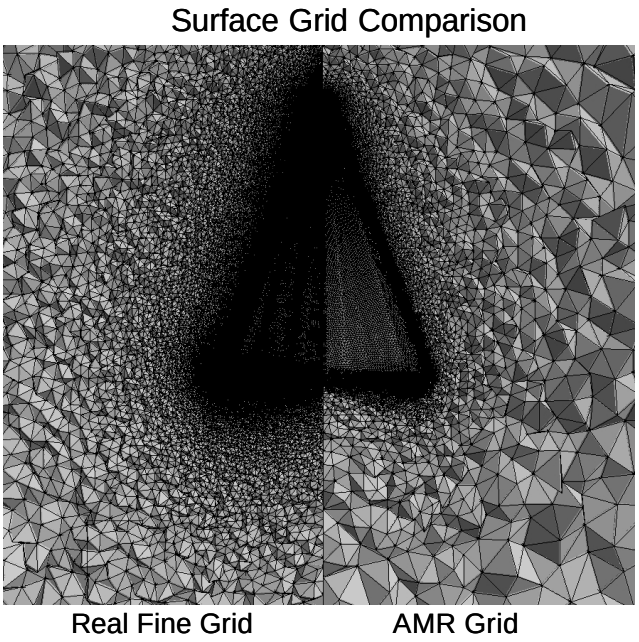

Fig. 8: Down-ward view of a longitudinal plane at the delta wing surface for real fine grid (10.7M cells) and the adaptive mesh refinement Grid (3.2M cells).

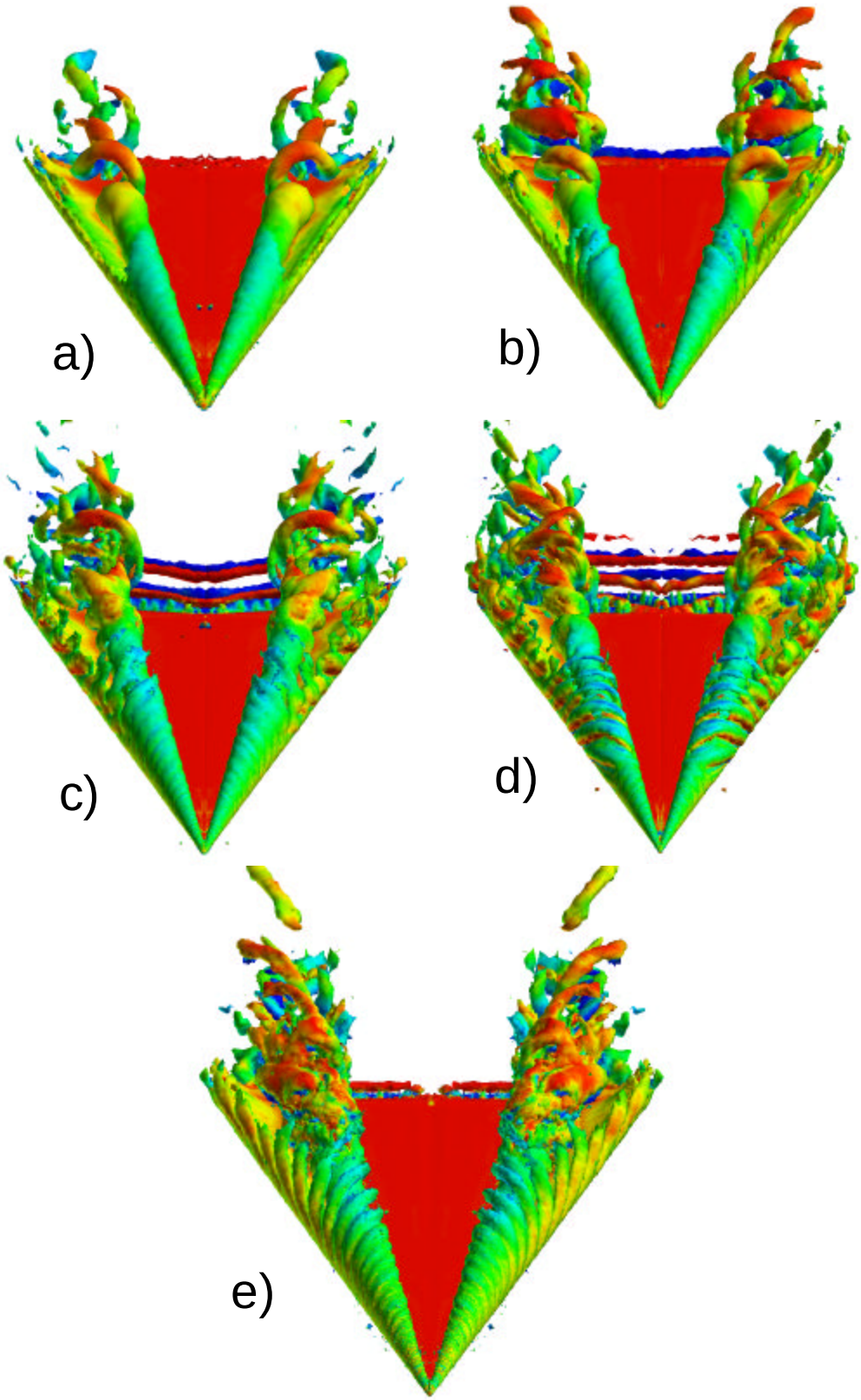

Fig. 9: Detached Eddy Simulation results of the 70° delta wing at $\alpha = 27°$ and $Re_c = 1.56x10^6$ for five different grids. Iso-surfaces of vorticity colored by spanwise vorticity component are presented. a) Coarse Grid-1.2M cells, b) Medium Grid-2.7M cells, c) Fine Grid-6.7M cells, d) Real Fine Grid-10.7M cells, e) Adavtive Mesh Refinement Grid-3.2M cells.

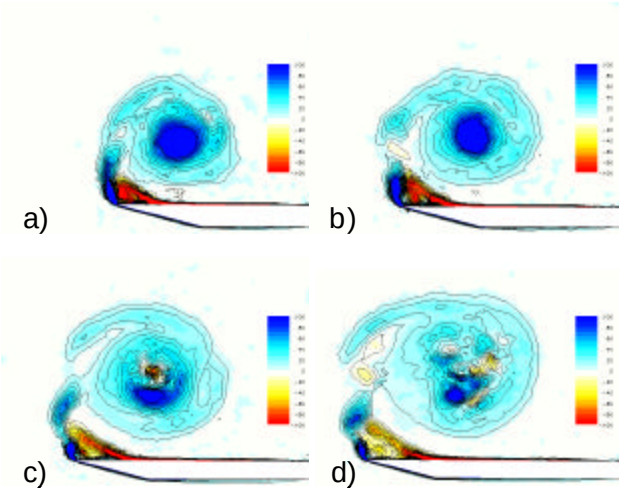

Fig. 10: Real Fine grid Detached Eddy Simulation results of instantaneous axial vorticity (Ω_x c/U_∞) at α = 27º and U_∞ = 24 m/s (a) X/c = 0.53 (500mm) (b) X/c = 0.63 (600mm) (c) X/c = 0.74 (700mm) (d) X/c = 0.84 (800mm).

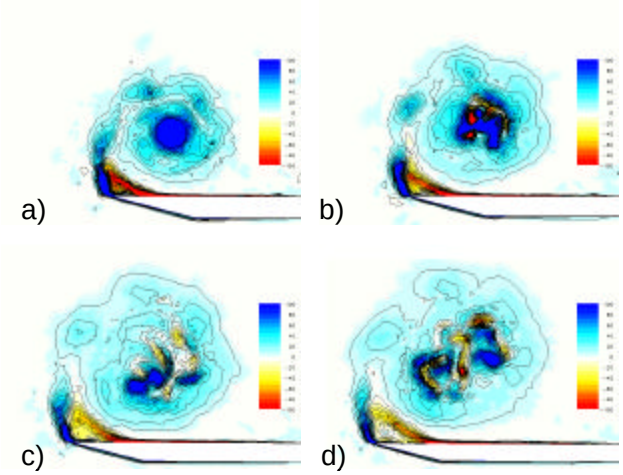

Fig. 11: AMR grid Detached Eddy Simulation results of instantaneous axial vorticity (Ω_x c/U_∞) at α = 27º and U_∞ = 24 m/s (a) X/c = 0.53 (500mm) (b) X/c = 0.63 (600mm) (c) X/c = 0.74 (700mm) (d) X/c = 0.84 (800mm).

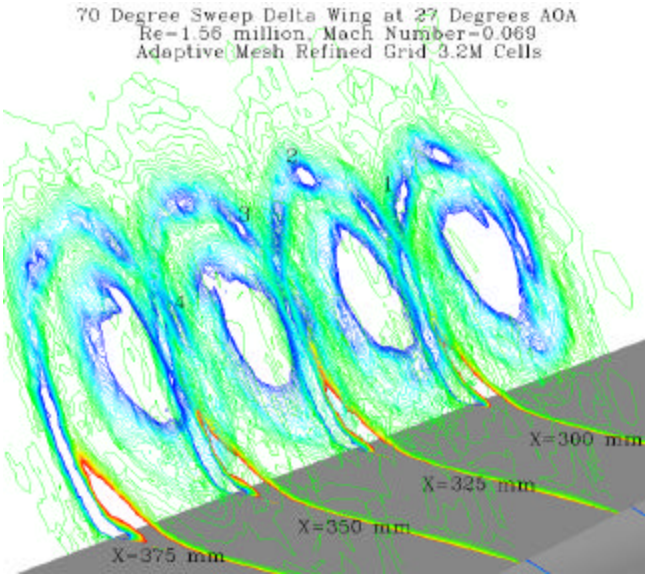

Fig. 12: Cross-planes of vorticity at four streamwise stations (300mm, 325mm, 350mm, and 375mm) for the AMR grid Detached Eddy Simulation demonstrating the vortical substructures captured with CFD.

[1] Délery, J., "Physics of Vortical Flows," *Journal of Aircraft*, Vol. 29, No. 5, Sept-Oct 1992, pp. 856-876.
[2] Werlé, H., "Sur l'éclatement des tourbillons," ONERA Note Technique No. 175, Nov. 1971.
[3] Hall, M.G., "Vortex Breakdown", *Annual Review of Fluid Mechanics*, Vol. 4, 1972, pp. 195-218.
[4] Leibovich, S., "The Structure of Vortex Breakdown," *Annual Review of Fluid Mechanics*, Vol. 10, 1978, pp. 221-46.
[5] Sarpkaya, T. "On Stationary and Traveling Vortex Breakdowns," *Journal of Fluid Mechanics*, Vol. 45, Part 3, 1971, pp. 545-559.
[6] Nelson, R.C., "Unsteady Aerodynamics of Slender Wings," *Aircraft Dynamics at High Angles of Attack: Experiments and Modeling*, AGARD-R-776, 1991, pp.1-1 to 1-26.
[7] Visbal, M.R., "Computational and Physical Aspects of Vortex Breakdown on Delta Wings," AIAA Paper 95-0585, Jan. 1995.
[8] Délery, J., "Aspects of Vortex Breakdown," *Progress in Aerospace Sciences*, Vol. 30, 1994, pp. 1-59.
[9] Gad-El-Hak, M. and Blackwelder, R.F., "The Discrete Vortices from a Delta Wing," *AIAA Journal*, Vol. 23, No. 6, June 1985, pp. 961-962.
[10] Reynolds, G. and Abtahi, A., "Three Dimensional Vortex Development, Breakdown and Control," AIAA Paper 89-0998, March 1989.
[11] Gordnier, R.E., "Computation of a Kelvin-Helmholtz Instability for Delta Wing Vortex Flows," WL-TR-91-3098, Flight Dynamics Directorate, Wright Laboratory, Wright-Paterson AFB, OH, Nov. 1991.
[12] Gordnier, R.E., "Computational Study of a Turbulent Delta-Wing Flowfield using Two-Equation Turbulence Models" AIAA Paper 96-2076, June 1996.
[13] Squire, H.B., Jones, J.G. and Stanbrook, A., "An Experimental Investigation of the Characteristics of some Plane and Cambered 65 Deg Delta Wings at Mach Numbers from 0.7 to 2.0," ARC, *R&M* No. 3305, 1961.
[14] Payne, F.M., Ng, T.T., Nelson, R.C. and Schiff, L.B., "Visualization and Wake Surveys of Vortical Flow over a Delta Wing," *AIAA Journal*, Vol. 26, No. 2, Feb. 1988, pp. 137-143.
[15] Lowson, M.V., "Visualization Measurements of Vortex Flows," AIAA Paper 89-0191, Jan. 1989.
[16] Verhaagen, N.G., Meeder, J.P. and Verhelst, J.M., "Boundary Layer Effects of the Flow of a Leading-Edge Vortex," AIAA Paper 93-3463, Aug. 1993.
[17] Washburn, A.E. and Visser, K.D., "Evolution of Vortical Structures in the Shear Layer of Delta Wings," AIAA Paper 94-2317, June 1994.
[18] Lowson, M.V., Riley, A.J. and Swales, C., "Flow Structure over Delta Wings," AIAA Paper 95-0586, Jan. 1995.
[19] Honkan, A. and Andreopoulos, J., "Instantaneous Three-Dimensional Vorticity Measurements in Vortical Flow over a Delta Wing," *AIAA Journal*, Vol. 35, No. 10, Oct. 1997, pp.1612-1620.
[20] Ng, T.T. and Oliver, D.R., "Leading-Edge Vortex and Shear Layer Instabilities," AIAA Paper 98-0313, Jan. 1998.
[21] Ho, C.M. and Huerre, P., "Perturbed Free Shear Layer," *Annual Review of Fluid Mechanics*, Vol. 16, 1984, pp. 365-424.
[22] Molton, P., "Etude expérimentale de l'éclatement tourbillonnaire sur aile delta en écoulement incompressible: caractérisation du champ externe", ONERA RT 53/1147AN, 1992.
[23] Mitchell, A.M., "Caractérisation et contrôle de l'éclatement tourbillonnaire sur une aile delta aux hautes incidences," Ph.D. Thèse, Université de Paris 6, Département de Mécanique, Juillet 2000.
[24] Mitchell, A.M. and Molton, P., "Vortical Substructures in the Shear Layers Forming Leading-Edge Vortices", AIAA Paper 2001-2424, June 2001.
[25] Spalart, P. R., and Allmaras, S.R., "A One Equation Turbulence Model for Aerodynamic Flows," *La Recherche Aerospatiale*, 1994, 1, p.5.
[26] Barberis, D., "Test Cases for CFD Validation," ONERA TP No. 1993-161, 1993.
[27] Strang, W.Z., Tomaro, R.F., Grismer, M.J., "The Defining Methods of Cobalt: A Parallel, Implicit, Unstructured Euler/Navier-Stokes Flow Solver," AIAA 99-0786, January 1999.
[28] Strelets, M., "Detached Eddy Simulation of Massively Separated Flows," AIAA 01-0879, January 2001.
[29] Morton, S.A., Forsythe, J.R., Mitchell, A.M., and Hajek, D., "DES and RANS Simulations of Delta Wing Vortical Flows," AIAA 2002-0587, January 2002.
[30] Forsythe, J.R., Hoffmann, K.A., Dieteker, F.F., "Detached-Eddy Simulation of a Supersonic Axisymmetric Base Flow with an Unstructured Flow Solver," AIAA 00-2410, June 2000.
[31] Shur, M., Spalart, P.R., Strelets, M., and Travin, A., 1999, "Detached Eddy Simulation of an Airfoil at High Angle of Attack," 4th International Symposium of Engineering Turbulence Modelling and Measurements, Corsica, May 24-26, 1999.
[32] Samareh, J., "Gridtool: A Surface Modeling and Grid Generation Tool," Proceedings of the Workshop on Surface Modeling, Grid Generation, and Related Issues in CFD Solution, NASA CP-3291, May 9-11, 1995.
[33] Pirzadeh, S., "Progress Toward A User-Oriented Unstructured Viscous Grid Generator," AIAA Paper 96-0031, January 1996.
[34] Pirzadeh, S., ``Vortical Flow Prediction Using an Adaptive Unstructured Grid Method", Research & Technology Organization Applied Vehicle Technology Panel Meeting, Norway, 7-11 May 2001.